Optical Fiber Technology 87 (2024) 103929

Contents lists available at ScienceDirect

Optical Fiber Technology

journal homepage: www.elsevier.com/locate/yofte

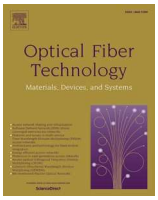

Regular Articles

# Tapered fiber optic sensor for arterial pulse wave monitoring

Sang-Woo Seo *, Noguosadia Egharevba

*Department of Electrical Engineering, City College of New York, New York 10031, NY, USA*

ARTICLE INFO

*Keywords:*
Tapered fiber sensor
Arterial pulse wave monitoring
Health monitoring systems

ABSTRACT

Arterial pulse wave monitoring has been recognized as an effective medical diagnostic tool for various cardiovascular diseases. To overcome the barriers in traditional, complex, and expensive detection configurations, new electronic and optical sensors have been developed with their unique advantages. Particularly, various configurations of fiber-optic sensors have been proposed. This paper demonstrates the use of a tapered optical fiber structure to create a sensitive sensor that can detect carotid arterial pulse waves on the skin surface. The demonstrated fiber sensor probe utilizes an in-line Mach-Zehnder interferometer configuration and liquid-gold film coating on the sensor tip to enhance its sensitivity and demonstrate its use by encapsulating the sensor with a flexible elastomer material for detecting arterial pulse waves with a simple testing configuration. Considering the simple fabrication and high sensitivity without a complex demodulation scheme, the proposed sensor has broad implementation in biomedical health monitoring systems.

## 1. Introduction

Arterial pulse waves (APWs) result from the abrupt rise in blood pressure from the cardiac ejection and its interaction with the distensible artery walls [1]. The rhythmic APWs propagate through the blood vessels and are measurable on various skin surfaces. The physical heart condition and arterial elastic properties certainly affect the pulse waveforms and rates, which are important vital signatures of human health conditions. Many studies have shown a close correlation between health status and the properties of arterial pulse waves [2–4]. For example, the measurements of APW velocities were used to diagnose peripheral vascular diseases and cardiovascular health [2]. The arterial elasticity indicated some links in hypertension and arteriosclerosis [5–7]. Variations in arterial pulse waveforms implicated clinical signs of vascular diseases [2,8,9]. The clinical importance of noninvasive APW measurements has drawn a lot of interest in the various sensors for monitoring APWs. As personalized healthcare is getting more and more popular at home, low-cost sensors are introduced to detect APWs and other vital signals from traditional, complex, expensive system configurations [10–12]. Flexible APW sensors based on emerging nanomaterials have been studied by examining the relationship between their electrical properties and the applied strain [13–16]. Novel piezoresistive and piezoelectric materials are introduced to electronic sensors. Compared with electronic sensors, optical sensors are generally bulky and expensive but provide alternative merits of utilizing approaches to achieve high sensitivity and can be used in certain severe environments due to their chemical stability and immunity to electromagnetic interference. In particular, optical fiber-based sensors are widely researched [17,18]. Generally, mechanical signals resulting from APWs on skin surfaces are investigated through intensity, wavelength, or phase modulation in fiber-based sensors. Intensity modulation-based sensors use relatively simple instrumental configurations with limited sensitivities. For example, a reflective diaphragm-based sensor has been demonstrated to measure deflection caused by arterial distension [19]. Wavelength modulation schemes are most commonly utilized with sensors based on Fiber-Bragg grating [20–23]. However, to improve their sensitivities, they require additional amplification schemes and relatively expensive interrogation systems to track the Bragg wavelength shifts. Finally, the phase modulation scheme has been implemented in an interferometer configuration, which provides high sensitivity but requires additional demodulation techniques to accurately retrieve displacement signals [24,25].

In this paper, we present a tapered-fiber optical sensor that uses an interferometric-assisted intensity modulation scheme to detect APWs. While various tapered fiber optic sensors are traditionally used on strain monitoring [26–28] or bio-chemical sensing applications [29–31], there are few reports of tapered fiber optical sensors to detect arterial pulses for human health monitoring. Furthermore, the typical configuration of using the optical transmission in tapered fiber sensors is not convenient for routine, portable APW monitoring applications. We designed a

* Corresponding author.
*E-mail address:* swseo@ccny.cuny.edu (S.-W. Seo).

https://doi.org/10.1016/j.yofte.2024.103929
Received 8 June 2024; Received in revised form 11 July 2024; Accepted 25 July 2024
Available online 30 July 2024

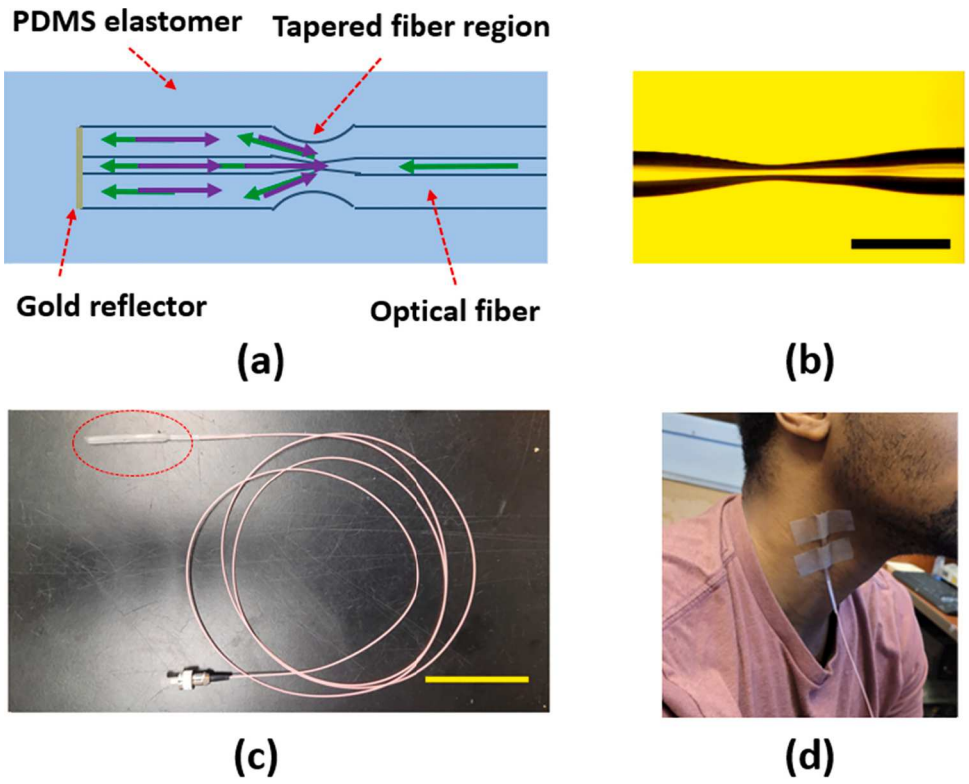


**Fig. 1.** (a) Schematic design of a tapered-fiber sensor encapsulating with PDMS elastomer. (b) An example image of a tapered fiber region (0.25 mm scale bar). (c) An image of a fabricated sensor probe (50 mm scale bar). (d) Implementation of a sensor to measure arterial pulse waves.

reflection-type fiber sensor probe utilizing an in-line Mach-Zehnder interferometer configuration to enhance its sensitivity and demonstrate its stable use by encapsulating the sensor with a flexible elastomer material for detecting APWs with a simple testing configuration. Considering the simple fabrication and high sensitivity without a complex demodulation scheme, the proposed sensor has a broad implementation on real-time health monitoring systems.

## 2. Design and fabrication

Fig. 1(a) shows the schematic design of our fiber sensor probe to detect APWs on a target skin surface. The sensor probe is formed with a tapered fiber structure encapsulated by flexible Polydimethylsiloxane (PDMS) elastomer. The sensor has a reflection-type construction with a gold reflection mirror at the tip to enable remote handheld usage of the sensor. Fig. 1(b) shows an example of the tapered region of a fiber sensor. Fig. 1(c) shows an example image of a fabricated fiber sensor probe. The red circle area indicates the PDMS-encapsulated tapered fiber sensor. It can be applied to detect APWs on the skin surface at the neck (Fig. 1(d)) or wrist using simple adhesive tapes. The detection mechanism is based on optical power modulation due to the fiber bending near the tapered region, which is caused by skin-surface displacement through the rhythmic expansion of an artery. Particularly, the presented structure utilizes an in-line Mach-Zehnder interference structure to enhance its displacement sensitivity. A portion of the optical mode in the core is excited to higher-order clad modes as a result of the fiber core diameter being reduced by employing the tapered fiber structure. The interference pattern with the core mode is the result of the clad modes being linked back to the core after being reflected off the tip gold reflector. Small pressure or displacement applied on the tapered region and the remaining fiber structure disrupts the power coupling and phase difference, resulting in optical signal modulation. The theoretical expression for the interference signal can be formulated as given below [32]:

$$I = (I_{core} + \sum_m I_{clad}^m + \sum_m 2\sqrt{I_{core} \times I_{clad}^m} \times \cos\Phi_d^m) \times R$$

where $I$, $I_{core}$ and $I_{clad}^m$ represent the intensity of the interference signal, the intensity guided through the core, and the intensity guided through m-th clad mode, respectively. $R$ presents the reflection coefficient at the fiber tip. Phase difference at an m-th clad mode is denoted as $\Phi_d^m = 4\pi \bullet (n_{eff}^{core} - n_{eff}^{m-clad}) \bullet \frac{L}{\lambda}$ Here, $L$ represents the length of the in-line MZI structure from the tip to the tapered region. $n_{eff}^{core}$ and $n_{eff}^{m-clad}$ are the effective refractive indices of the core and m-th cladding mode, respectively. $\lambda$ represents the signal wavelength in vacuum. When multiple clad modes exist, the spectral characteristics of the interference signal reflect the overlap of multiple mode interferences. The large intensity contrast is expected to be observed when $I_{core}$ and $I_{clad}^m$ have similar intensities with a single dominant cladding mode. In the reflection-type configuration with PDMS coating, $R$ will be less than 1 % without any additional reflection coating, given that the refractive index of PDMS at 1550 nm is around 1.4 [33]. Therefore, an effective reflection coating should be applied to increase the overall intensity of the interference signal, which is interfaced with an optical receiver. When a tapered fiber sensor is attached to the skin surface close to a blood vessel, the displacement caused by the arterial pulses puts a strain on the fiber to be bent. This will affect the optical power coupling of $I_{core}$ and $I_{clad}^m$, and the phase difference, $\Phi_d^m$ resulting in the intensity modulation at the interference signal. By calibrating the sensor at a particular wavelength with significant intensity changes, a low-cost APW monitoring sensor can be realized.

To fabricate the sensors, standard single-mode fibers with a core diameter of 9 μm, and a cladding diameter of 125 μm, were employed. After removing the plastic coating layer, the fiber was cleaned with isopropanol alcohol. One end of the fiber was cleaved, and the fiber was mounted onto a custom-built fiber splicer. The distance from the end of

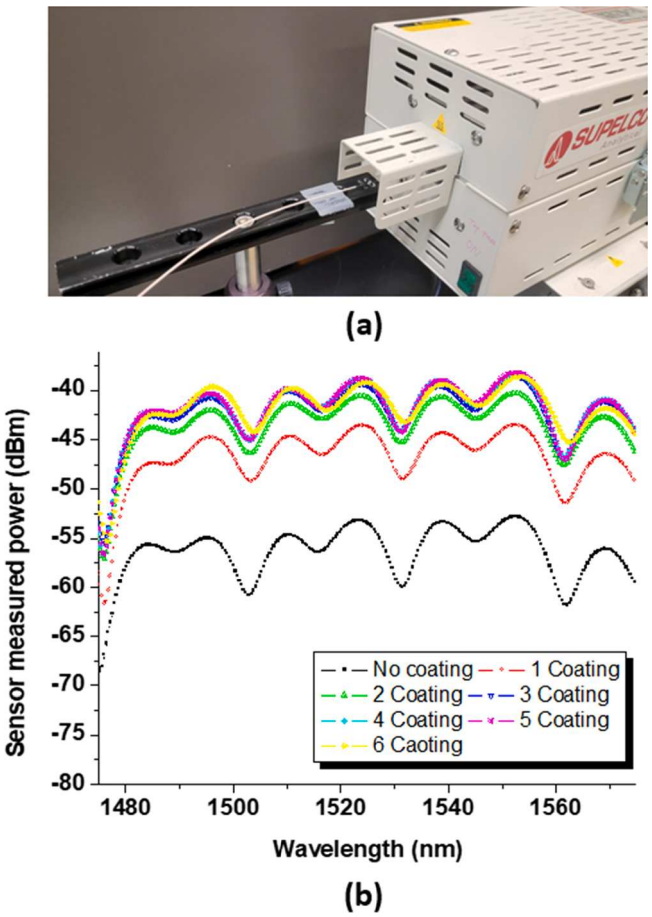


**Fig. 2.** (a) An image of the gold-coating process on tip of a fiber sensor in a tube furnace. (b) Reflected optical power spectrum as a function of gold-coating on the tip of a fabricated sensor.

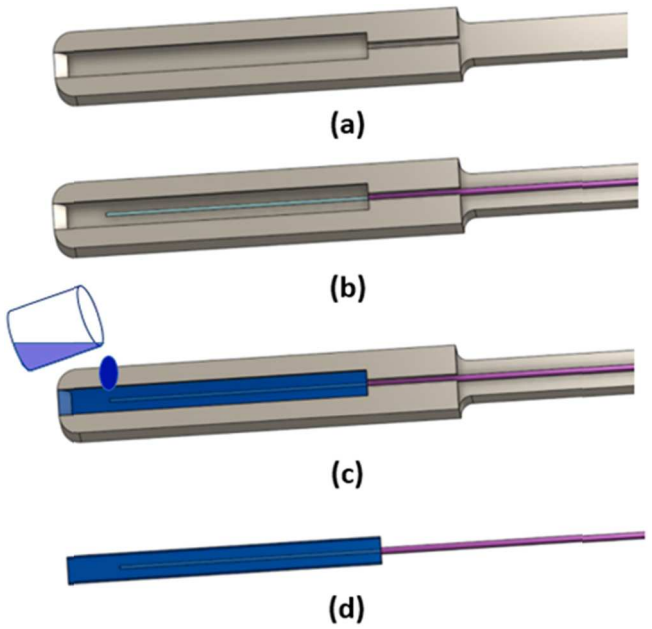


**Fig. 3.** Sensor embedding process in flexible PDMS elastomer material. (a) 3D-printed mold preparation. (b) Fiber sensor alignment within the 3D-printed mold. (c) PDMS pouring and curing. (d) Released sensor with PDMS elastomer layer.

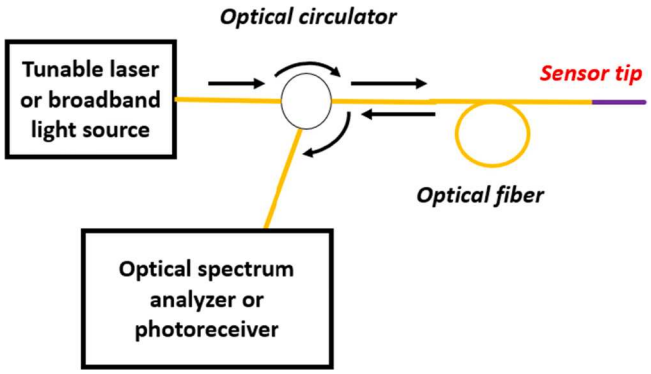


**Fig. 4.** Schematic diagram of a generalized measurement configuration.

the fiber to the tapered region was kept to around 1.5 cm. Typical tapering parameters include around 40 μm (minimum diameter) and 750 μm (length) of the tapered region, respectively. During the tapering process, the output signal of the sensor was monitored via an optical circulator with an optical spectrum analyzer and a broadband light source for resonance optimization. Following the tapering procedure, a thin layer of gold was formed on the tip of the fiber as an optical reflector. Using a liquid-based gold solution (GOLDFILM, Emulsitone Chemicals), we developed a simple coating method in place of the conventional vacuum deposition of a metal layer. The fiber tip section of the sensor was wetted using the gold solution and then placed inside a tube furnace, where it was dried for 15 min at 500 °C. The basic method to check the quality of the coating is to measure its reflected optical power instead of controlling the thickness of each coated layer. Once a tapered fiber structure is formed at a bare glass fiber, it is relatively delicate at this stage. Therefore, the fiber tip was dip-coated with gold solution without aggressive coating procedures. Fig. 2 shows an image of the gold-coating process in a tube furnace (Fig. 2(a)) and an example (Fig. 2(b)) of optical spectrum measurement of six repetitive coating and drying processes from the bare fiber sensor without gold coating. The measurement data shows that the reflected optical power is saturated after 3–4 layers of the sequential gold coating. This was fairly consistent with separate coating experiments in more than ten different trials. This reflection coating is important to ensure suitable optical reflection power from the sensor tip when it is embedded in the PDMS elastomer.

The next step is to embed the sensor in flexible PDMS elastomer material, which creates a protective layer of the delicate fiber structure during its use. Fig. 3 shows the sensor embedding process in flexible PDMS elastomer material. A 3D-printed mold structure was designed and created using polylactic acid-based material (Fig. 3(a)). First, a tapered fiber sensor was aligned with the 3D-printed mold structure (Fig. 3(b)). The Dow Corning Sylgard 184 elastomer kit was used to make a liquid PDMS mixture. A mixture of ten-parts base elastomer and one-part curing agent was prepared by vacuum-degassing. Subsequently, the prepared PDMS liquid mixture was poured and cured at 60 °C for 5 hrs (Fig. 3(c)). Finally, after the complete PDMS curing, the sensor with a protective PDMS layer was removed from the mold with a drop of isopropyl alcohol as a releasing agent (Fig. 3(d)).

## 3. Results and discussion

To understand the sensor characteristics, we have performed various sensor characterizations. Fig. 4 shows a generalized characterization setup to investigate the sensor's response as a function of dynamic and static displacement applied to the sensor. Either a tunable laser (Newfocus 6428) or a broadband light source (Thorlabs S5FC1550S) was used as a light source. The optical signal from a light source is coupled using an optical circulator to a fabricated tapered fiber sensor, where its mechanical motion modulates the optical signal. The resulting sensor

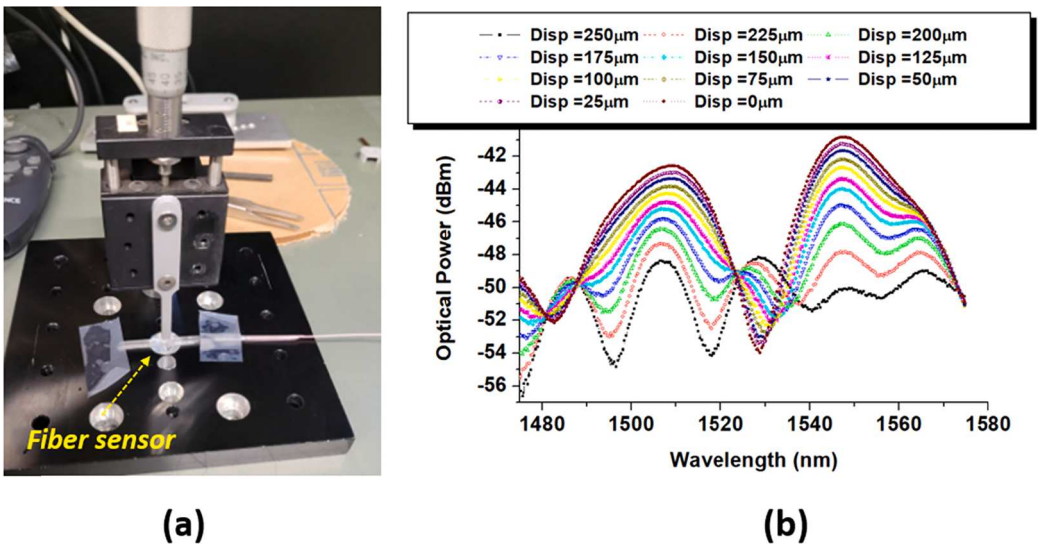


**Fig. 5.** Static characterization of a fabricated sensor. (a) A photo image of the measurement setup. (b) Measured static response of a fabricated sensor as a function of different displacements applied on the sensor.

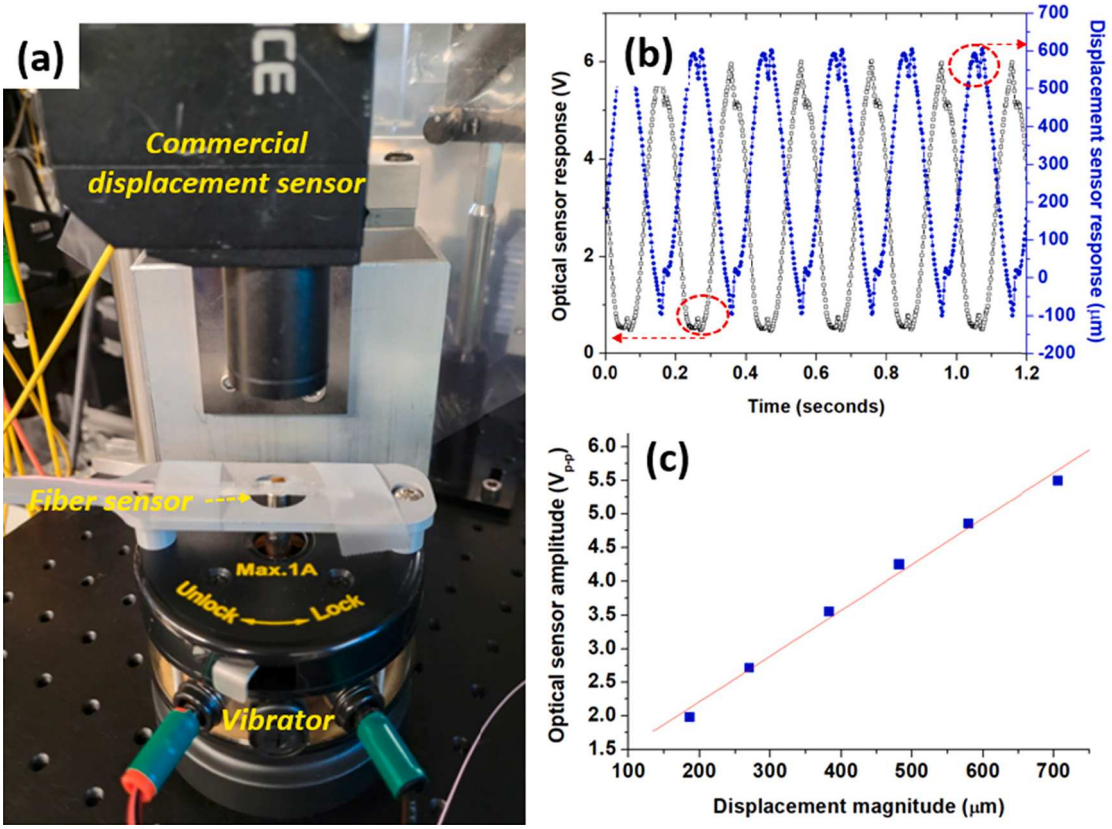


**Fig. 6.** Dynamic characterization of a fabricated sensor. (a) A photo image of the measurement setup. (b) Measured dynamic responses of a fabricated sensor and a commercial displacement sensor at 5 Hz vibration. (c) Measured optical sensor amplitude as a function of applied displacement magnitude.

output signal was measured using an optical spectrum analyzer (HP 70952B) or an amplified optical receiver (Thorlabs PDA400).

First, static sensor characteristics were studied when a constant displacement was applied to the sensor tapered region. Fig. 5(a) shows an experimental setup with a mounted fiber sensor. A taped sensor was mounted on a hole (8 mm diameter) of an aluminum platform. A 3D-printed stick with a 4 mm × 4 mm square tip was placed on a linear stage using a micrometer positioner to apply a relative displacement on the sensor tapered region. As expected from the in-line MZI configuration, the fiber sensor exhibits periodic interferometric resonances in its spectral response, as shown in Fig. 5(b). It was observed that the sensor was quite sensitive to how it was mounted on a test surface since the optical coupling at the tapered region was changed, and a strain-induced phase change was introduced in the response. Nevertheless, it was seen that the optical loss at the particular wavelength ranges due to the interferometric resonances was dominantly enhanced as the

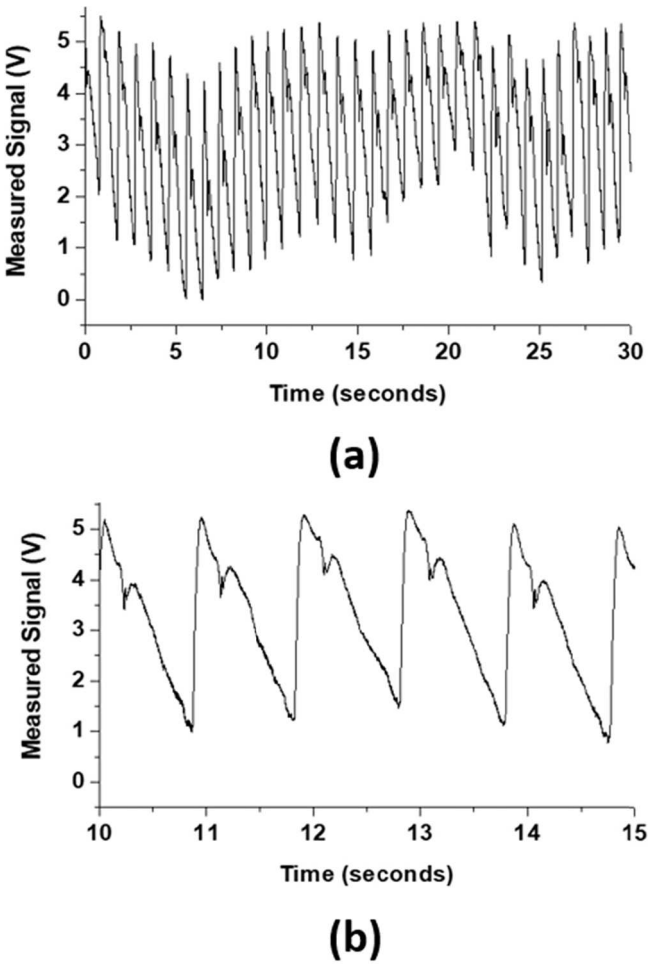


**Fig. 7.** Measured arterial pulse waves on the skin surface at the neck for 30 s duration (a) and zoomed pulse waveforms (b).

displacement increased.

To investigate the sensor dynamic characteristics, the sensor was mounted on a vibrator, as shown in Fig. 6(a). A center pin (7 mm in diameter) of the vibrator was positioned at the tapered region of the sensor. A constant vibration at a frequency of 5 Hz was applied to the sensor. At the same time, the displacement of the sensor surface was monitored using a commercial displacement sensor (Keyence LT-9031M). To improve the optical reflection for the commercial sensor, a small reflective tape (3 mm × 3 mm square) was attached to the top of the sensor surface. To measure the dynamic response of the sensor, the optical signal from the tunable laser was coupled to the sensor using an optical circulator, and its resulting optical signal was measured by an amplified photoreceiver. The signal from the photoreceiver was connected to a data acquisition system (eDAQ e-corder 410), where the measured signal was quantized and recorded with 0.312 mV resolution and 1000 samples/sec. During the measurement, the signal from the commercial displacement sensor was also acquired so that both signals could be compared. The wavelength of the tunable laser was set to 1545 nm since the sensor had wide optical intensity responses at around 1545 nm wavelength when displacement was applied based on the static measurement. Fig. 6(b) shows the measured responses from the commercial displacement sensor and our fabricated tapered fiber sensor. As expected from the static measurement, the more displacement introduced the higher loss, resulting in the response from our fiber sensor being revered from the response of the commercial displacement sensor. Otherwise, the fiber sensor signal agreed well with the signal from the commercial displacement sensor. This confirms that the fiber sensor can accurately measure the dynamic displacement applied on the sensor surface. Fig. 6(c) shows the sensor amplitude as a function of the measured displacement distance. Different displacements were applied to the sensor by changing the driver signal applied to the vibrator. The sensor response was quite linear within the displacement ranges that are expected from artery pulse measurements [34]. Based on the linear fit of the measured signal, 6.78 mV/μm sensitivity was obtained at the current setup with 0.312 mV acquisition resolution. Considering that the typical human pulse rate varies from around 60 to 100 pulses/min, the demonstrated sensor based on the calibration measurement at 5 Hz has enough bandwidth to capture the human arterial pulse responses.

Finally, the sensor was implemented to monitor artery pulse waves on the skin surface of the neck area. The fiber sensor was attached to the carotid artery vessel area at the neck using adhesive tapes. APWs were measured using a similar configuration to the dynamic response measurements of the sensor. Fig. 7 shows the measured responses for 30 s of duration (Fig. 7(a)) and its zoomed pulse shapes (Fig. 7(b)). The sensor signal was reversed to correctly follow the artery volume change, as discussed in the dynamic measurements. The measured individual signals represent similar artery pulse waves with early and late systolic peaks with dicrotic notches observed in other published papers [35,36]. Additionally, the baseline modulation seen in Fig. 7(a) indicates inhale and exhale of breathing patterns. It has been discussed that APWs are affected by various physical parameters of a human when the blood pressure waves travel from the heart to arterial vessels and indicate potential symptoms of cardiovascular malfunctions. The simple tapered fiber sensor is expected to be a low-cost, sensitive front-end device that can be interfaced with a healthcare monitoring system to quantify the vital signs of human health.

## 4. Conclusions

We presented a tapered optical fiber sensor that can be attached to the arterial blood vessel area and monitor arterial pulse waves. Low-cost fabrication of the sensor was presented using fiber tapering, gold solution-based reflector coating, and elastic PDMS encapsulation. Based on in-line MZI configuration, the fabricated sensor shows high sensitivity, which can distinguish skin-surface displacements within the ranges of arterial blood vessel volume changes. The comparison of the measurements from a fabricated sensor and a commercial displacement sensor confirmed that the proposed sensor could be used to detect dynamic displacements. The measurement from an adult human demonstrated that the sensor could successfully measure the detailed arterial pulse waveforms with breathing patterns. Due to its simple fabrication and implementation without any complex demodulation scheme, the presented sensor can be a real-time sensing element that can monitor arterial pulse waves and interface to general health monitoring systems.

## CRediT authorship contribution statement

**Sang-Woo Seo:** Conceptualization, Methodology, Supervision, Writing – original draft, Writing – review & editing. **Noguosadia Egharevba:** Methodology, Writing – review & editing.

## Declaration of competing interest

The authors declare that they have no known competing financial interests or personal relationships that could have appeared to influence the work reported in this paper.

## Data availability

Data will be made available on request.

## Acknowledgment

This work was supported by National Science Foundation grant (NSF-2324052).

## References

[1] J. Alastruey, P.H. Charlton, V. Bikia, B. Paliakaite, B. Hametner, R.M. Bruno, M. P. Mulder, S. Vennin, S. Piskin, A.W. Khir, Arterial pulse wave modeling and analysis for vascular-age studies: a review from VascAgeNet, Am. J. Physiol.-Heart Circ. Physiol. 325 (1) (2023) H1–H29.
[2] T. Kanda, E. Nakamura, T. Moritani, Y. Yamori, Arterial pulse wave velocity and risk factors for peripheral vascular disease, Eur. J. Appl. Physiol. 82 (2000) 1–7.
[3] B. Li, H. Gao, X. Li, Y. Liu, M. Wang, Correlation between brachial-ankle pulse wave velocity and arterial compliance and cardiovascular risk factors in elderly patients with arteriosclerosis, Hypertens. Res. 29 (5) (2006) 309–314.
[4] L. Qiao, Z. Qi, L. Tu, Y. Zhang, L. Zhu, J. Xu, Z. Zhang, The association of radial artery pulse wave variables with the pulse wave velocity and echocardiographic parameters in hypertension, Evid.-Based Complement. Altern. Med. 2018 (1) (2018) 5291759.
[5] F.W. Haynes, L.B. Ellis, S. Weiss, Pulse wave velocity and arterial elasticity in arterial hypertension, arteriosclerosis, and related conditions, Am. Heart J. 11 (4) (1936) 385–401.
[6] X. Liu, H. Gao, B. Li, M. Cheng, Y. Ma, Z. Zhang, X. Gao, Y. Liu, M. Wang, Pulse wave velocity as a marker of arteriosclerosis and its comorbidities in Chinese patients, Hypertens. Res. 30 (3) (2007) 237–242.
[7] H. Kim, S. Kim, Pulse wave velocity in atherosclerosis, Front. Cardiovasc. Med. 6 (2019) 41.
[8] J.N. Cohn, S. Finkelstein, G. McVeigh, D. Morgan, L. LeMay, J. Robinson, J. Mock, Noninvasive pulse wave analysis for the early detection of vascular disease, Hypertension 26 (3) (1995) 503–508.
[9] J. Allen, A. Murray, Comparison of three arterial pulse waveform classification techniques, J. Med. Eng. Technol. 20 (3) (1996) 109–114.
[10] A.L. Wentland, T.M. Grist, O. Wieben, Review of MRI-based measurements of pulse wave velocity: a biomarker of arterial stiffness, Cardiovasc. Diagn. Ther. 4 (2) (2014) 193.
[11] M. Couade, The advent of ultrafast ultrasound in vascular imaging: a review, J. Vasc. Diagn. Interven. (2016) 9–22.
[12] J. Doupis, N. Papanas, A. Cohen, L. McFarlan, E. Horton, Pulse wave analysis by applanation tonometry for the measurement of arterial stiffness, Open Cardiovasc. Med. J. 10 (2016) 188.
[13] Q. Sun, C. Yeung, H. Chan, W.J. Li, A.L.R. Vellaisamy, Nanomaterials for flexible arterial pulse sensors, in Soft Matter and Biomaterials on the Nanoscale: The WSPC Reference on Functional Nanomaterials—Part I Volume 4: Nanomedicine: Nanoscale Materials in Nano/Bio Medicine Anonymous World Scientific, 2020, pp. 309–359.
[14] B.H. Moghadam, M. Hasanzadeh, A. Simchi, Self-powered wearable piezoelectric sensors based on polymer nanofiber–metal–organic framework nanoparticle composites for arterial pulse monitoring, ACS Appl. Nano Mater. 3 (9) (2020) 8742–8752.
[15] M. Kim, I. Doh, E. Oh, Y. Cho, Flexible piezoelectric pressure sensors fabricated from nanocomposites with enhanced dispersion and vapor permeability for precision pulse wave monitoring, ACS Appl. Nano Mater. 6 (23) (2023) 22025–22035.
[16] S.N.A. Ismail, N.A. Nayan, M. Haniff, M.A. Shazni, R. Jaafar, Z. May, Wearable two-dimensional nanomaterial-based flexible sensors for blood pressure monitoring: a review, Nanomaterials 13 (5) (2023) 852.
[17] R. Jha, P. Mishra, S. Kumar, Advancements in optical fiber-based wearable sensors for smart health monitoring, Biosens. Bioelectr. (2024) 116232.
[18] C. Perezcampos Mayoral, J. Gutiérrez Gutiérrez, J.L. Cano Pérez, M. Vargas Treviño, I.B. Gallegos Velasco, P.A. Hernández Cruz, R. Torres Rosas, L. Tepech Carrillo, J. Arnaud Ríos, E.L. Apreza, Fiber optic sensors for vital signs monitoring. A review of its practicality in the health field, Biosensors 11 (2) (2021) 58.
[19] C.S.J. Leitão, da Costa Antunes, P. Fernando, J.A. Bastos, J. Pinto, de Brito André, P. Sérgio, Plastic optical fiber sensor for noninvasive arterial pulse waveform monitoring, IEEE Sens. J. 15 (1) (2014) 14–18.
[20] R.B. Gowda, P. Sharan, K. Saara, M. Braim, A.N. Alodhayb, An FBG-based optical pressure sensor for the measurement of radial artery pulse pressure, J. Biophoton. (2024) e202400083.
[21] S. Padma, S. Umesh, T. Srinivas, S. Asokan, Carotid arterial pulse waveform measurements using fiber Bragg grating pulse probe, IEEE J. Biomed. Health Inf. 22 (5) (2017) 1415–1420.
[22] B.S. Kavitha, S. Pant, A.K. Sood, S. Asokan, Fiber grating sensors and their recent applications in biomedical domain, J. Opt. (2023).
[23] D. Jia, J. Chao, S. Li, H. Zhang, Y. Yan, T. Liu, Y. Sun, A fiber Bragg grating sensor for radial artery pulse waveform measurement, IEEE Trans. Biomed. Eng. 65 (4) (2017) 839–846.
[24] J.E. Posada-Román, M. Ruiz-Llata, P. Acedo, J.A. Garcia-Souto, J. Bezares, "Fetal heart beat monitor using a fiber laser interferometric sensor: A preliminary study on the detection of the signals, IEEE Sens. 2017 (2017) 1–3.
[25] N.A. Ushakov, A.A. Markvart, L.B. Liokumovich, Pulse wave velocity measurement with multiplexed fiber optic Fabry-Pérot interferometric sensors, IEEE Sens. J. 20 (19) (2020) 11302–11312.
[26] F.J. Arregui, I.R. Matías, M. López-Amo, Optical fiber strain gauge based on a tapered single-mode fiber, Sensors Actuat. A: Phys. 79 (2) (2000) 90–96.
[27] C. Zhang, T. Ning, J. Zheng, J. Xu, X. Gao, H. Lin, J. Li, L. Pei, An optical fiber strain sensor by using of taper based TCF structure, Opt. Laser Technol. 120 (2019) 105687.
[28] K. Tian, M. Zhang, G. Farrell, R. Wang, E. Lewis, P. Wang, Highly sensitive strain sensor based on composite interference established within S-tapered multimode fiber structure, Optics Express 26 (26) (2018) 33982–33992.
[29] F. Liu, W. Zhang, X. Lang, X. Liu, R. Singh, G. Li, Y. Xie, B. Zhang, S. Kumar, Development of taper-in-taper-based optical fiber sensors for chemical and biological sensing, Photonics (2023) 567.
[30] S. Korposh, S.W. James, S. Lee, R.P. Tatam, Tapered optical fibre sensors: Current trends and future perspectives, Sensors 19 (10) (2019) 2294.
[31] Y. Li, Z. Xu, S. Tan, F. Fang, L. Yang, B. Yuan, Q. Sun, Recent advances in microfiber sensors for highly sensitive biochemical detection, J Phys. D 52 (49) (2019).
[32] Y. Li, E. Harris, L. Chen, X. Bao, Application of spectrum differential integration method in an in-line fiber Mach-Zehnder refractive index sensor, Optics Express 18 (8) (2010) 8135–8143.
[33] V. Prajzler, P. Nekvindova, J. Spirkova, M. Novotny, The evaluation of the refractive indices of bulk and thick polydimethylsiloxane and polydimethyl-diphenylsiloxane elastomers by the prism coupling technique, J. Mater. Sci.: Mater. Electron. 28 (2017) 7951–7961.
[34] S. Casaccia, E.J. Sirevaag, E.J. Richter, J.A. O'Sullivan, J.W. Rohrbaugh, Features of the non-contact carotid pressure waveform: Cardiac and vascular dynamics during rebreathing, Rev. Sci. Instrum. 87 (10) (2016).
[35] J.W. Cunningham, P. Di Achille, V.N. Morrill, L. Weng, S.H. Choi, S. Khurshid, V. Nauffal, J.P. Pirruccello, S.D. Solomon, P. Batra, Machine learning to understand genetic and clinical factors associated with the pulse waveform dicrotic notch, Circulation: Genomic Precision Med. 16 (1) (2023) e003676.
[36] R. Pal, A. Rudas, S. Kim, J.N. Chiang, A. Braney, M. Cannesson, An algorithm to detect dicrotic notch in arterial blood pressure and photoplethysmography waveforms using the iterative envelope mean method, medRxiv, 2024.